





SCIENTIFIC REPORTS



OPEN

Metabolites and Lipids Associated with Fetal Swine Anatomy via Desorption Electrospray Ionization – Mass Spectrometry Imaging

Marisol León¹ , Christina R. Ferreira², Livia S. Eberlin³, Alan K. Jarmusch⁴ , Valentina Pirro², Ana Clara Bastos Rodrigues¹ , Phelipe Oliveira Favaron⁵, Maria Angelica Miglino¹ & R. Graham Cooks² 

Chemical imaging by mass spectrometry (MS) has been largely used to study diseases in animals and humans, especially cancer; however, this technology has been minimally explored to study the complex chemical changes associated with fetal development. In this work, we report the histologically-compatible chemical imaging of small molecules by desorption electrospray ionization (DESI) - MS of a complete swine fetus at 50 days of gestation. Tissue morphology was unperturbed by morphologically-friendly DESI-MS analysis while allowing detection of a wide range of small molecules. We observed organ-dependent localization of lipids, *e.g.* a large diversity of phosphatidylserine lipids in brain compared to other organs, as well as metabolites such as N-acetyl-aspartic acid in the developing nervous system and N-acetyl-L-glutamine in the heart. Some lipids abundant in the lungs, such as PC(32:0) and PS(40:6), were similar to surfactant composition reported previously. Sulfatides were highly concentrated in the fetus liver, while hexoses were barely detected at this organ but were abundant in lung and heart. The chemical information on small molecules recorded via DESI-MS imaging coupled with traditional anatomical evaluation is a powerful source of bioanalytical information which reveals the chemical changes associated with embryonic and fetal development that, when disturbed, causes congenital diseases such as spina bifida and cleft palate.

Molecular and anatomical features are intertwined. Yet they are often studied independently of each other, largely because of limitations in the available analytical tools. Animal models are essential to understanding disease including the development of new therapies in translational medicine. Since there are numerous anatomical, physiological and molecular similarities between pigs and humans and because pigs are frequently used as a source for organ transplantation¹, studying pig ontogeny is an attractive choice for developmental biology research.

Lipids play an important role in cellular physiology and are implicated in developmental diseases such as type I diabetes^{2,3}, Niemann–Pick diseases^{4,5} and Gaucher's disease^{5,6}. The physiological consequences of disrupting the genes responsible for lipid metabolism are often severe developmental problems including alterations in neural development, muscular dystrophy, bone deformity, cartilage developmental problems, altered respiratory system development, gonadal and reproductive dysfunctions, liver failure, and embryonic lethality^{7–13}. The role of small metabolites and the processes which govern their formation, distribution, and roles are equally important and critical for proper anatomical and physiological development.

Mass spectrometry (MS) imaging is one method that provides spatial as well a chemical information – bridging the gap between anatomy and physiology. This combination allows acquisition of comprehensive morphological and chemical data and has the potential to contribute to lowering the number of animals needed in research. Desorption

¹Surgery Department, School of Veterinary Medicine and Animal Science, University of Sao Paulo, Sao Paulo, Brazil. ²Department of Chemistry and Center for Analytical Instrumentation Development, Purdue University, West Lafayette, IN, 47907, United States. ³Department of Chemistry, The University of Texas at Austin, Austin, TX, 78712, United States. ⁴Collaborative Mass Spectrometry Innovation Center, Skaggs School of Pharmacy and Pharmaceutical Sciences, University of California San Diego, La Jolla, CA, 92093, United States. ⁵State University of Londrina, Londrina, Paraná, 86051-990, Brazil. Correspondence and requests for materials should be addressed to R.G.C. (email: cooks@purdue.edu)

electrospray ionization – mass spectrometry (DESI-MS) is a matrix-free and simple chemical imaging method that can be used to map small molecules in unmodified tissue sections. In a DESI-MS imaging experiment, a spray of charged solvent droplets rasters across the surface of a sample (such as a tissue section placed on a glass slide) and molecules are dissolved in the solvent spot forming a microfilm. The DESI spray is accelerated by a nitrogen gas stream which drives the solvent droplets towards the sample. The subsequent droplets impact the liquid spot and release secondary microdroplets containing the desorbed molecules and direct them to the inlet of the mass spectrometer where solvent evaporates generating free gas-phase ions^{14–16}. The application of DESI-MS to tissue analysis benefits from the use of histologically-compatible solvent combinations, such as acetonitrile and dimethylformamide mixed at equal amounts. Such solvents maintain tissue integrity and cell morphology when used as the spray solvent in the DESI-MS analysis¹⁷. Morphologically-friendly DESI-MS imaging is used to profile metabolites and lipids present in tissue samples without disturbing the tissue morphology¹⁷. The preservation of morphology allows morphological information to be combined with data on the same tissue as is analyzed by DESI-MS^{18,19}.

Lipid profiling and imaging, i.e. untargeted lipid detection and relative quantification, has been explored by DESI-MS and matrix-assisted laser desorption ionization (MALDI) MS in bovine, mouse, fish and swine animal species. However, these studies were restricted either to early embryonic stages (preimplantation) or to embryonic uterine implantation^{16,20–29}. The use of the DESI-MS imaging for whole body analysis has been reported by Perez *et al.*³⁰ to describe the location of toxic ionic liquids in specific areas of adult zebrafish. DESI-MS has allowed mapping of the location at 2D and 3D spatial domain for a wide range of lipid species such as free fatty acids (FFA), glycerophospholipids, glycerolipids and sphingolipids^{22,31}.

In this research, we apply morphologically-friendly DESI-MS imaging combined with optical microscopy to characterize the location of FFA and some phosphatidylcholine (PC), phosphatidylserine (PS), sulfatide (ST), and phosphatidylinositol (PI) lipids in the whole body of two swine fetuses at an advanced stage of development (around day 50) when organogenesis can be observed. The location of selected molecules was studied in the 2D and 3D images. Since the lipid composition during mammalian organogenesis is largely unexplored, our findings were correlated with small molecule imaging reported for cells and organs. Lipids and metabolites concentrated in specific organs are pointed out since these may have key roles for the establishment of physiological function. As examples, palmitic acid, oleic acid, PC(36:1)/PE(40:4), and PE(40:3) were present in all organs. The nervous system showed high abundances of an array of specific PI and PS lipids while sulfatides were mostly detected in the gastrointestinal system. N-acetyl-L-glutamic acid was detected only in the heart, and N-acetyl-aspartate was specifically located in the brain tissue. To our knowledge, this is the first study describing the location of lipids and metabolites at an advanced stage of fetal development. DESI-MS imaging is highly applicable to understanding complex developmental processes and should be useful to study developmental diseases.

Material and Methods

Chemicals. When not otherwise stated, reagents were purchased from Sigma-Aldrich (St. Louis, MO). All reagents were HPLC grade (OmniSolv®).

Samples. The experimental workflow is summarized in Fig. 1. For DESI-MS experiments, two frozen swine fetuses around day 50 of pregnancy were obtained from a commercial supplier (Animal Technologies, Inc.). No institutional committee is reported for this research since the biological samples used in the experiments were sold as frozen samples by Animal Technologies, Inc. No handling of live vertebrates occurred and therefore the experiments did not require approval from the Purdue Animal Care and Use Committee (PACUC). The samples were frozen and embedded in optimal cutting temperature (OCT) compound for slicing 15- μm thick sections using a cryotome (Shandon SME Cryotome cryostat GMI, Inc., Ramsey, MN, USA). Whole body sections were mounted onto plain glass slides (Erie Scientific, Portsmouth, NH). No fixative agents were used before or after slicing. After sectioning, the samples were stored at -80°C until analysis, when they were dried in a desiccator for ~ 15 min. All DESI-MS experiments were performed at Purdue University, IN.

DESI-MS imaging and data analysis. Experiments were carried out in the negative ion mode by applying a -5 kV spray voltage to the needle of the syringe used to deliver the spray solvent³². Dimethylformamide-acetonitrile (1:1) (*v/v*) solvent was sprayed at the rate of 1.5 $\mu\text{L}/\text{min}$ under 180 psi of nebulizing gas (N_2) pressure. Mass spectra were acquired from *m/z* 150 to 1,000 from different sections representing the whole swine fetus body. The DESI spray was at an incident angle of 51° to the surface plane and *circa* 2 mm distant from the instrument inlet. The DESI spray emitter consisted of an inner capillary with an inner diameter (ID) of 50 μm and outer diameter (OD) of 150 μm , and an outer capillary with an ID of 250 μm and an OD of 350 μm . The mass spectrometer used was an LTQ linear ion trap controlled by Xcalibur 2.0 software (Thermo Fisher Scientific, San Jose, CA, USA). Tissues were scanned using a lab-built 2D moving stage with horizontal rows separated by a vertical step of 300 μm . An in-house program allowed the conversion of the XCalibur 2.0 mass spectra files (.raw) into a format compatible with Biomap (freeware, <http://www.maldi-msi.org>), in which spatially resolved images were assembled and displayed in the interpolated mode. Ion images were independently normalized to 100 and displayed using a color-coded scale. The lipid species were putatively identified by MS/MS and by high mass resolution obtained by manually directing the DESI spray onto specific organs using an Orbitrap mass spectrometer (Exactive, Thermo Scientific, San Jose, CA, USA). After DESI-MS imaging, the whole-body tissue sections were stained with H&E and morphological images were manually overlaid with the DESI-MS ion images. Biomap (Novartis, Basel, Switzerland) was used for the visualization of 2D ion images, and a MATLAB-based data processing routine was used for 3D mass spectrometry imaging³¹. Due to the wealth of molecular location information acquired by DESI-MS imaging, not all data could be presented in this manuscript. The authors will gladly share all data upon request.

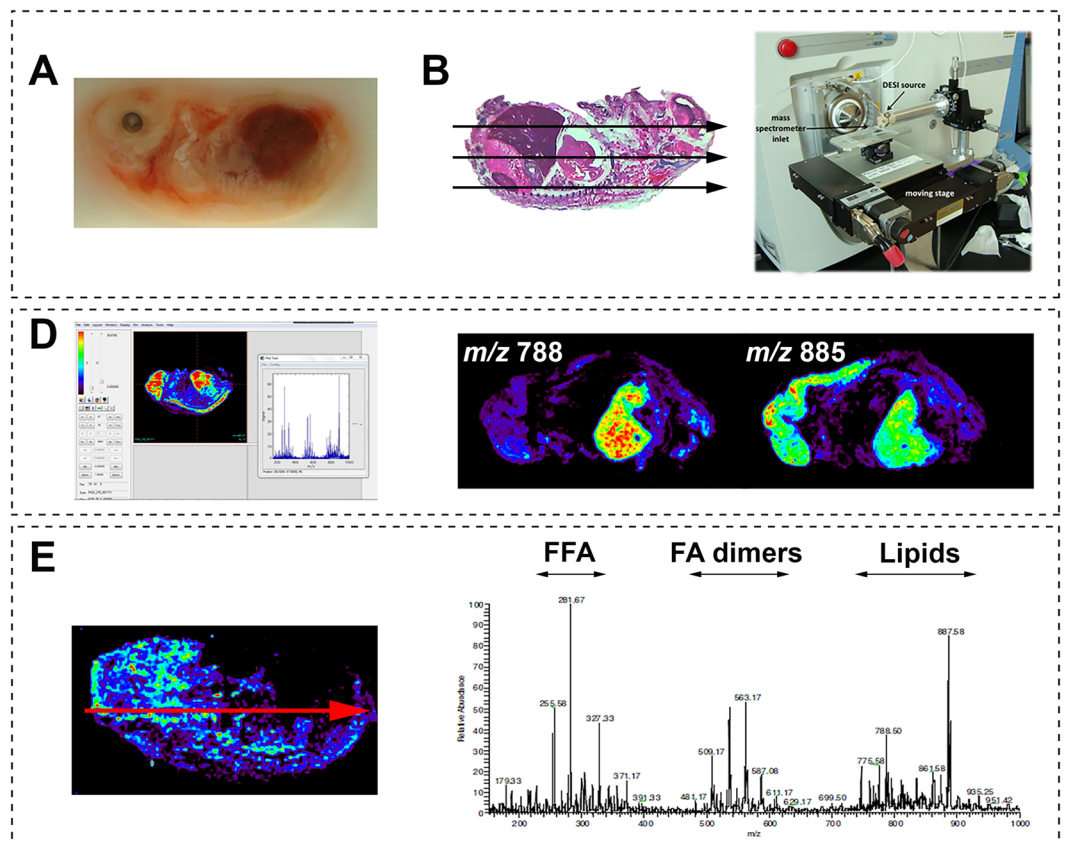


Figure 1. Workflow of DESI-MS imaging of a whole swine fetus. (A) Samples were sectioned using a cryotome and mounted onto glass slides. The whole swine fetus volume was sectioned using 300 μm of lateral resolution (Fig. S1). Glass slides were stored at $-80\text{ }^{\circ}\text{C}$ and before analysis were thawed and placed in a desiccator for ~ 15 min. (B) DESI-MS images were acquired in an ion trap mass spectrometer equipped with an in-house built moving stage. (C) Ion images were visualized using BioMAP 3.7.5.5 provided by Novartis Institutes for BioMedical Research (freeware). (D) Spectral data were averaged across an entire line of an ion image (red line) and the resulting DESI-MS mass spectrum was displayed, showing the mass-to-charge (m/z) range.

Results

Macroscopic evaluation was used to determine gestational age. Swine fetuses used for this study had 37 mm of crown-rump indicating a gestational age of approximately 50 days³². Organogenesis stage was determined by morphology as described elsewhere³³ and supported by the complete formation of the eyes, heart, brain, lungs, liver, stomach, and kidneys. Further evaluation revealed cephalic regions, eyes with pigmented retinas, upper and lower eyelids, external ears, and limbs with keratinized and separated digits. Additional details on the morphological evaluation are shown in Figs S2 and S3.

The DESI-MS imaging experiment was used to visualize the 2D and 3D molecular anatomy of the fetus associated with developmental processes (see discussion). The lateral resolution used was 300 μm , which allowed most of the organs to be evident while maintaining a reasonable data acquisition of 3 h for the largest whole-body 2D image. The 3D volumetric distribution included 2D images of 45 tissue sections (longitudinal sections spaced by an average of 160 μm) of one of the swine fetuses. The imaging experiment is not destructive, allowing for posthoc histopathology and co-registration of chemical and morphological information (Fig. 2).

Figure 3 displays as example the location in 3D of the FA dimer C16:0 and C18:1, m/z 537, overlaid with the location of PS(36:1), m/z 788. Higher ion abundances for the FA dimer were found in the liver and the pro-encephalic mass (diencephalon and telencephalon) of the nervous system as well as in the intestines, while the PS(36:1) is distributed volumetrically throughout the entire body except the intestines. The creation of 3D images from the 2D DESI images illustrates the power of MS imaging for morphological and developmental studies, providing complementary chemical whole-body mapping. The 3D visualization provides information on how the compound distribution changes over the body volume. Examples of 3D reconstruction from 2D images by DESI-MS data are shown by Eberlin *et al.* (2010) and Xiong *et al.* (2012) for mouse brain^{31,34}. Dueñas *et al.* (2017) reported 3D zebrafish imaging by MALDI-MS²⁸.

Table 1 lists a set of lipids and metabolites that were detected in the nervous system (brain and spinal cord), cardiopulmonary system (heart and lungs), gastrointestinal and urinary systems (liver, intestines, and kidneys). The lipids were detected in negative ion mode, mostly as deprotonated ions $[\text{M} - \text{H}]^-$ with the exception of phosphatidylcholines (PCs) and ceramides that were detected as chlorinated adducts $[\text{M} + \text{Cl}]^-$ ³⁵. Other lipids classed included phosphatidylserines (PS), sulfatides (ST), phosphatidylinositols (PI), sphingomyelin (SM), and FFA, all

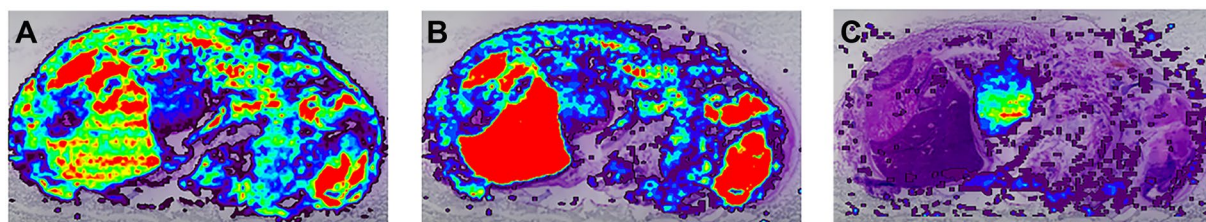


Figure 2. Overlay of 2D DESI-MS image and post-hoc H&E stain. (A) m/z 215; (B) m/z 885; and (C) m/z 788.

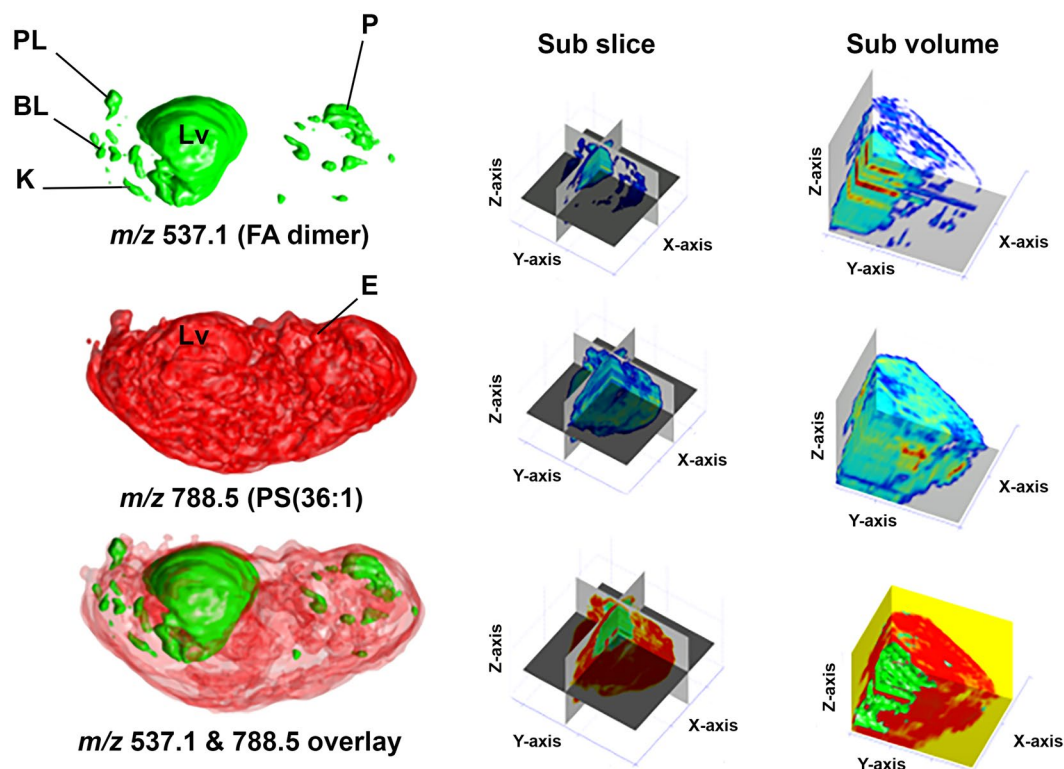


Figure 3. 3D mass spectrometry images of C18:1 and C16:0 FA dimer (m/z 537), and of PS(36:1) m/z 788 generated by aligning 2D ion images of 45 tissue sections to illustrate the distribution of these molecules in the whole fetus. These images were obtained using the software package described previously³¹. Legend: (Lv) Liver, (P) Prosencephalon, (PL) Pelvic limb, (BL) Blowel loops, (K) Kidney, (E) Eye.

of which have structural and signaling roles in cells. Illustrative mass spectra for each organ are shown in Fig. 4. Putative metabolite and lipid annotations were based on DESI-MS literature, tandem MS and high-resolution MS data (Table 1, Fig. S4). Figures 5 and 6 depict ion images of selected lipids and their differential distribution in 2D throughout the swine fetus. Ion intensities in the images are color-coded and scaled to 100. Intensities are scaled independently in each ion image to optimize the contrast and facilitate comparison with morphological distribution.

Discussion

Lipid and metabolite composition of the swine fetal nervous system. The nervous system, particularly the brain, has been extensively studied using mass spectrometry imaging (DESI and MALDI). The lipid composition of the brain presents some difference between species^{36,37}, but it is nominally consistent within each species. The nervous system displayed a great variety of metabolites, illustrated in Figs 5 and 6. Among those that stand out arachidonic acid (C20:4, Fig. S4), stearic acid (C18:0), PG(34:1; Fig. S4), and PS(36:1) were also identified by MALDI-MS during mouse embryo uterine implantation²⁰.

Other metabolites identified in the brain such as palmitoleic acid (C16:1), palmitic acid (C16:0), oleic acid (C18:1), and PI(38:4) (Figs 5 and 6), besides the arachidonic acid (C20:4) they have also been previously identified by I DESI-MS in the brains of adult rats³⁸. We also detected fatty acids such as linoleic acid (C18:2) and eicosatrienoic acid (C20:3), which have been related to the differentiation and proliferation of neuronal cells, and with the synaptic development and peripheral neuropathies in humans³⁹. The swine fetus showed differential

Identification	Ion	Chemical formula (Ion)	Theoretical mass	Measured mass	Mass Error (ppm)
N-acetyl-aspartate	[M - H] ⁻	C ₆ H ₈ NO ₅	174.03981	174.03981	0
Ascorbic acid	[M - H] ⁻	C ₆ H ₇ O ₆	175.02371	175.02385	0.8
C6 sugar	[M - H] ⁻	C ₆ H ₁₁ O ₆	179.05501	179.05515	0.8
N-acetyl-glutamine	[M - H] ⁻	C ₇ H ₁₁ N ₂ O ₄	187.07133	187.07122	0.6
Palmitoleic acid	[M - H] ⁻	C ₁₆ H ₂₉ O ₂	253.21621	253.21644	0.9
Palmitic acid	[M - H] ⁻	C ₁₆ H ₃₁ O ₂	255.23186	255.23208	0.9
Linoleic acid	[M - H] ⁻	C ₁₈ H ₃₁ O ₂	279.23186	279.23201	0.5
Oleic acid	[M - H] ⁻	C ₁₈ H ₃₃ O ₂	281.24751	281.24766	0.5
Stearic acid	[M - H] ⁻	C ₁₈ H ₃₅ O ₂	283.26316	283.26332	0.6
EicosaPentaenoic acid	[M - H] ⁻	C ₂₀ H ₂₉ O ₂	301.21621	301.21630	0.3
Arachidonic acid	[M - H] ⁻	C ₂₀ H ₃₁ O ₂	303.23186	303.23195	0.3
Eicosatrienoic acid	[M - H] ⁻	C ₂₀ H ₃₃ O ₂	305.24751	305.24758	0.2
Eicosadienoic acid	[M - H] ⁻	C ₂₀ H ₃₅ O ₂	307.26327	307.26316	-0.4
DHA (ω-3)	[M - H] ⁻	C ₂₂ H ₃₁ O ₂	327.23186	327.23187	0.03
DPA (ω-3)	[M - H] ⁻	C ₂₂ H ₃₃ O ₂	329.24751	329.24752	0.03
Eranthic acid (ω-6)	[M - H] ⁻	C ₂₂ H ₃₇ O ₂	333.27881	333.27883	0.1
FA dimer	[M - H] ⁻	—	—	509.1*	—
FA dimer	[M - H] ⁻	—	—	535.2*	—
FA dimer	[M - H] ⁻	—	—	537.2*	—
FA dimer	[M - H] ⁻	—	—	563.2*	—
FA dimer	[M - H] ⁻	—	—	611.3*	—
FA dimer	[M - H] ⁻	—	—	699.3*	—
Cer(d34:1)	[M + Cl] ⁻	C ₃₄ H ₆₇ NO ₃ Cl	572.48040	572.47970	-1.2
Cer(d36:1)	[M + Cl] ⁻	C ₃₆ H ₇₁ NO ₃ Cl	600.51170	600.51102	-1.1
Cer(d42:2)	[M + Cl] ⁻	C ₄₂ H ₈₁ NO ₃ Cl	682.58995	682.58907	-1.3
PEP(34:1)	[M - H] ⁻	C ₃₉ H ₇₅ NO ₇ P	700.52752	700.52698	-0.8
PEP(36:4)	[M - H] ⁻	C ₄₁ H ₇₃ NO ₇ P	722.51192	722.51191	-0.01
PEP(36:2)	[M - H] ⁻	C ₄₁ H ₇₇ NO ₇ P	726.54322	726.54281	-0.6
PE(36:2)	[M - H] ⁻	C ₄₁ H ₇₇ NO ₈ P	742.53813	742.53745	-0.9
PG(34:1)	[M - H] ⁻	C ₄₀ H ₇₆ O ₁₀ P	747.51706	747.51626	-1.1
PeP(38:4)	[M - H] ⁻	C ₄₃ H ₇₇ NO ₇ P	750.54322	750.54249	-1.0
PeP(38:3)	[M - H] ⁻	C ₄₃ H ₇₉ NO ₇ P	752.55887	752.55796	-1.2
PS(34:1)	[M - H] ⁻	C ₄₀ H ₇₅ NO ₁₀ P	760.51231	760.51130	-1.3
PE(38:4)	[M - H] ⁻	C ₄₃ H ₇₇ NO ₈ P	766.53813	766.53727	-1.1
PE(38:3)	[M - H] ⁻	C ₄₃ H ₇₉ NO ₈ P	768.55379	768.55301	-1.0
PG(36:2)	[M - H] ⁻	C ₄₂ H ₇₈ O ₁₀ P	773.53271	773.53191	-1.0
PG(36:1)	[M - H] ⁻	C ₄₂ H ₈₀ O ₁₀ P	775.54836	775.54733	-1.3
PS(36:2)	[M - H] ⁻	C ₄₂ H ₇₇ NO ₁₀ P	786.52796	786.52708	-1.1
PS(36:1)	[M - H] ⁻	C ₄₂ H ₇₉ NO ₁₀ P	788.54361	788.54267	-1.2
PC(34:0)	[M + Cl] ⁻	C ₄₂ H ₈₂ NO ₈ P	794.54611	794.54508	-1.2
PS(38:4)	[M - H] ⁻	C ₄₄ H ₇₇ NO ₁₀ P	810.52796	810.52690	-1.3
PS(38:3)	[M - H] ⁻	C ₄₄ H ₇₉ NO ₁₀ P	812.54361	812.54272	-1.1
PS(38:2)	[M - H] ⁻	C ₄₄ H ₈₁ NO ₁₀ P	814.55926	814.55942	0.2
PG(40:6)	[M - H] ⁻	C ₄₆ H ₇₈ O ₁₀ P	821.53271	821.53160	-1.4
PS(40:6)	[M - H] ⁻	C ₄₆ H ₇₇ NO ₁₀ P	834.52796	834.52698	-1.2
PS(40:4)	[M - H] ⁻	C ₄₆ H ₈₁ NO ₁₀ P	838.55926	838.55841	-1.0
PS(40:3)	[M - H] ⁻	C ₄₆ H ₈₃ NO ₁₀ P	840.57491	840.57402	-1.1
PI(36:4)	[M - H] ⁻	C ₄₅ H ₇₈ O ₁₃ P	857.51746	857.51626	-1.4
PI(36:3)	[M - H] ⁻	C ₄₅ H ₈₀ O ₁₃ P	859.53186	859.53311	1.5
PI(36:2)	[M - H] ⁻	C ₄₅ H ₈₂ O ₁₃ P	861.54876	861.54809	-0.8
PI(36:1)	[M - H] ⁻	C ₄₅ H ₈₄ O ₁₃ P	863.56358	863.56441	1.0
ST(h22:0)	[M - H] ⁻	C ₄₆ H ₈₈ NO ₁₂ S	878.60217	878.59859	-4.1
PI(38:5)	[M - H] ⁻	C ₄₇ H ₈₀ O ₁₃ P	883.53311	883.53185	-1.4
PI(38:4)	[M - H] ⁻	C ₄₇ H ₈₂ O ₁₃ P	885.54876	885.54757	-1.3
PI(38:3)	[M - H] ⁻	C ₄₇ H ₈₄ O ₁₃ P	887.56441	887.56371	-0.8
(3'-sulfo)Gal3-Cer(d18:1/24:1(2OH))	[M - H] ⁻	C ₄₈ H ₉₀ NO ₁₂ S	904.61782	904.6*	—
(3'-sulfo)Gal3-Cer(d18:1/24:0(2OH))	[M - H] ⁻	C ₄₈ H ₉₂ NO ₁₂ S	906.63297	906.63347	0.6

Table 1. DESI high resolution mass spectral data and tentative identifications. *Measured in low resolution using a linear ion trap mass spectrometer.

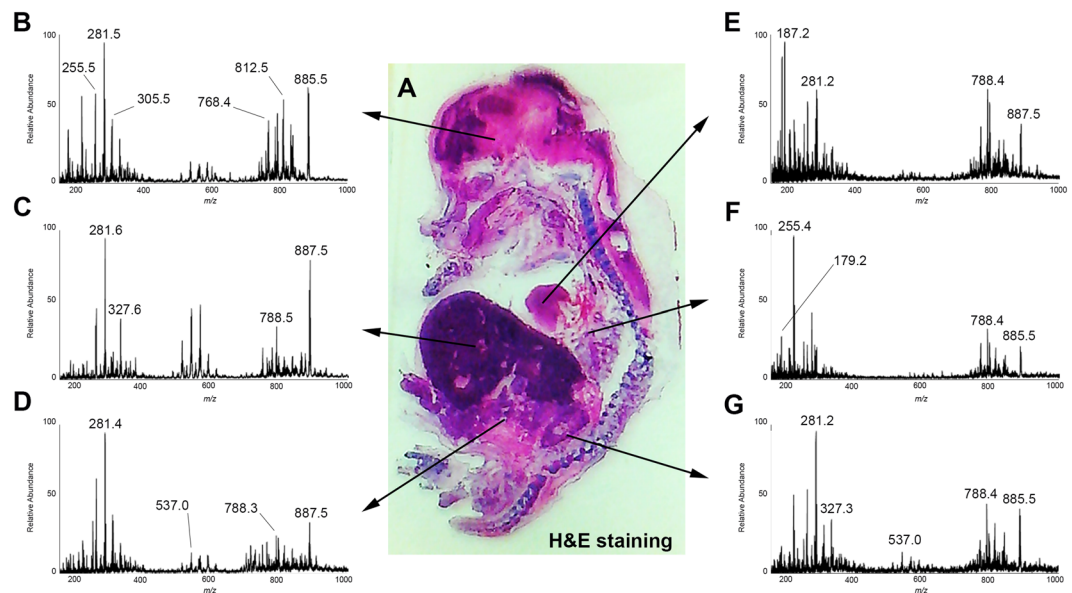


Figure 4. Representative mass spectra of some of the organs (indicated in the same H&E stained tissue section used for the DESI-MS imaging) and selected ion images. (A) H&E; (B) brain; (C) liver; (D) intestine; (E) heart; (F) lungs; (G) kidney.

distribution of PI lipids, such as PI(34:1), PI(38:3) and PI(38:4) through the different organs, but overall these lipids were more abundant at the nervous system and liver (Fig. 5). Burnum *et al.*²⁰ correlated the location of PI lipids during mouse embryonic implantation with the differentiation and proliferation of cells in the mouse embryo (rearrangement of the cytoskeleton, trafficking of intracellular vesicles). Girod *et al.*⁴⁰ detected differential distribution of PI(38:4) and PS(36:1) by DESI-MS in the areas of brain white and gray matter and in the spinal cord of the adult mice.

N-Acetyl-aspartate (NAA) of m/z 174 was most abundant in the nervous system compared to the other organs (Figs 6; S4). NAA is the second most concentrated molecule in the brain after the amino acid glutamate²⁶. This metabolite has been detected in the human and murine brain tissue and can be used as a biomarker of healthy brain tissue when imaging brain tumors^{26,41}. Roles for NAA include neuronal osmoregulation and axon-glia signaling, brain nitrogen balance⁴². Two human inborn errors are related to NAA metabolism: Canavan disease in which there is a buildup of NAA and associated spongiform leukodystrophy, caused by a lack of aspartoacylase activity. The later is a human condition where lack of NAA where the enzyme that synthesizes NAA is absent⁴³. Differences in lipid abundances were identified for the brain and spinal cord. The brain showed higher abundances than the spinal cord for ascorbic acid (Fig. 6), DHA (C22:6), PC(36:1)/PE(40:4), PC(32:0)/PE(38:3), PE(40:3), PEp(40:6), PG(40:6), PI(38:4), PS(40:4) and PS(40:6) (Fig. 5). DHA has been reported as the predominant fatty acid in the central nervous system and the retina in humans. It is also essential for the optimal functional maturation of retina and visual cortex, as well as in neural development⁴⁴. DHA level decrease has been linked in aging with diseases such as dementia and Alzheimer's disease³⁹. Also FA dimers of m/z 509, m/z 535, m/z 537, m/z 563 and PA(36:2) of m/z 699 (Fig. 6) were noticeably more present in the brain than in the spinal cord. FA dimers are formed during the desorption/ionization process and are not endogenous species in the tissue. Their abundance in the mass spectrum is proportional to the quantity of free FA in the tissue^{45,46}. The role of PIs in the nervous system lies in the formation of the neurite and the neural circuit⁴⁷ and the development of dendrites and the neuronal synapses⁴⁸.

Overall, the nervous system showed high abundances for six out of seven PS lipids observed, which may be related to neuronal apoptosis, a key mechanism in brain organogenesis^{12,13}. Specifically PS(38:3) and PS(40:4) have been associated with human brain tumors by Eberlin *et al.*⁴⁹ using DESI-MS and this is an interesting finding since glioblastoma tumorigenesis has been related to cellular dedifferentiation at embryological states⁵⁰.

Lipid and metabolite composition of the swine cardiopulmonary system. Hexoses were more evident in the heart than in other organs and barely detected in liver (Fig. 5). N-Acetyl-glutamine was strikingly abundant in the heart compared to any other organ (Fig. 6). The concentration of N-acetyl-glutamine in cardiac tissue may be related to the enzymatic activity of acetyl kinase in this organ. The absence of this enzyme causes atrophy and cardiac muscle weakness⁵¹. To our knowledge this is the first time that N-acetyl-glutamine has been reported to be concentrated in the developing heart tissue compared to other parts of the body.

Overall, the lipids of highest abundance for the lungs were PS(36:1) and PC(32:0)/PE(38:3) (Fig. 5). Some of the lipids present at the lungs could relate to the pulmonary surfactant beginning to be synthesized at this time of fetal development. Specifically PS is important for lung maturation and to prevent the collapse of alveoli in

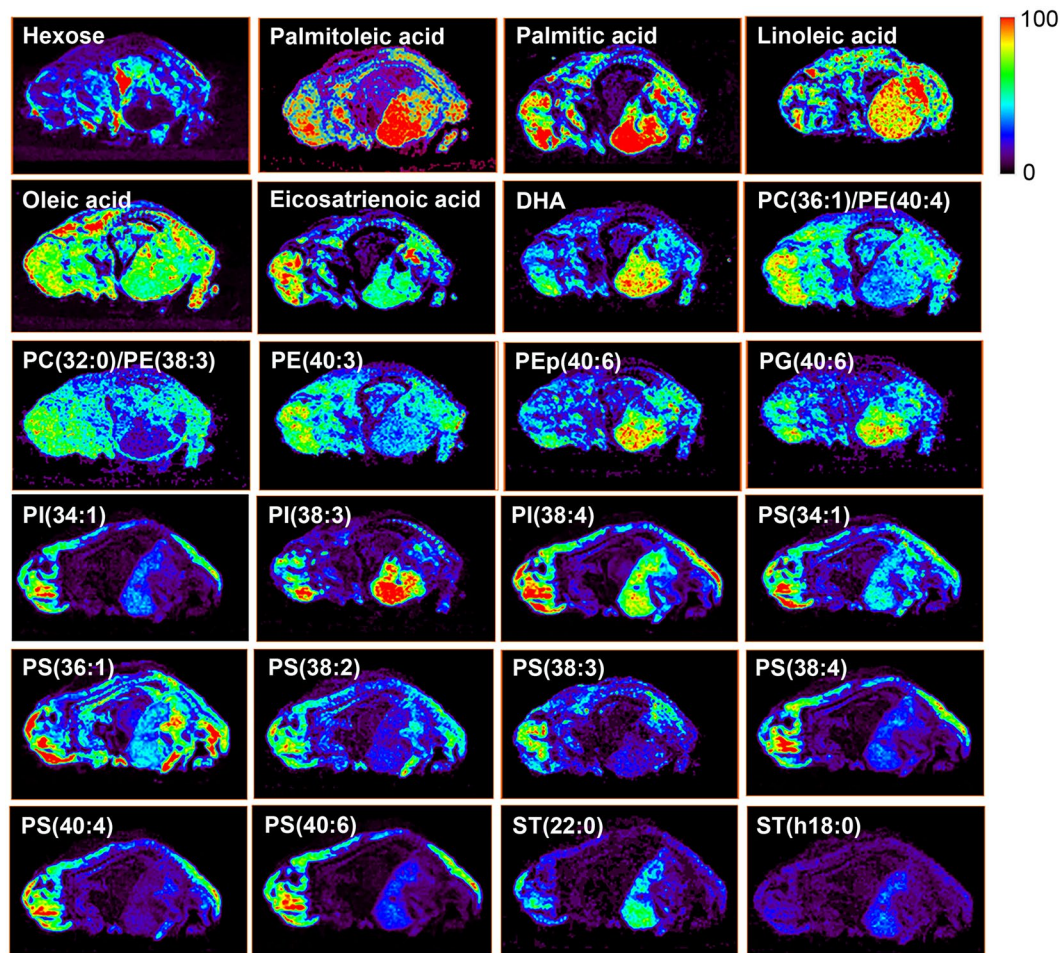


Figure 5. Ion images of selected metabolites and lipids distributed in the whole swine fetus body. Abundance in each ion image is independently scaled to 100 using the jet color-scale. Attributions are listed in Table 1. All ions are deprotonated versions of the molecules, viz. $[M - H]^-$, except for PC lipids which were detected as chlorine adducts $[M + Cl]^-$ in negative ion mode^{63,64}.

expiration^{52,53}. According to Sozo *et al.*⁵⁴, pulmonary surfactant is composed mostly of phospholipids such as PC(32:0), PC(36:1), PI(34:1), PI(38:3), PS(36:1) and PS(40:6). So except for PI(34:1) and PS(40:6), all these lipids were detected in the swine fetal lungs. Interestingly, swine and human surfactants show similar compositions and this fact has allowed the use of swine surfactant for the treatment of hyaline membrane disease in preterm newborns^{55–57}.

Lipid and metabolite composition of the swine fetus gastrointestinal and urinary system. The liver showed the highest abundances in the fetal body of the FA dimers of m/z 509, m/z 535, m/z 537 and m/z 611 (Fig. 6). PI(34:1), PI(38:4) and PA(36:2) were detected in the pig fetuses liver and also were reported in pig oocytes by DESI-MS^{23,28}. In addition, PI(38:4) and PA(36:2) are considered biomarkers of connective tissue and hepatic parenchyma respectively, being identified in dogs and human liver by MALDI-MS imaging⁵⁸.

The intestines were unique for PEp(36:2), PEp(36:4) and ST(h22:0) (Fig. 6). PI(36:4) was also detected in the intestines but absent in the renal system. Inglese *et al.*⁵⁹ identified PG(40:6) of m/z 821 and PI(38:4) of m/z 885 (Fig. S4) in human colorectal adenocarcinoma biopsies by 3D-DESI-MS.

Ascorbic acid, palmitic (C16:0), palmitoleic (C16:1), stearic (C18:0), oleic (C18:1), linoleic (C18:2), stearic (C18:1), arachidonic (C20:3), and eicosatrienoic (C20:4) acids (Figs 5 and 6) were detected in the kidneys at high ion abundances; and the glycerophospholipids such as PG(40:6), PI(34:1), PI(38:3), PI(38:4), PS(34:1), and PS(36:1) (Fig. 5) were also detected in the kidneys²². Dill *et al.* (2010) mapped PI(38:4) and PS(36:1) in human renal cell carcinomas⁶⁰. Pirro *et al.* (2012) reported the presence of PI(38:4) and PS(36:1) as markers of cancer in human bladder, kidney, germ cells and prostate cancer. We were not able to observe fully developed adrenal glands in porcine fetuses, but the lipids we observed were also identified with high abundances in the adult pig adrenal glands using DESI-MS⁶¹. Other lipids such as PI(34:1), PG(34:1) have been associated with human cell carcinomas using DESI-MS⁶².

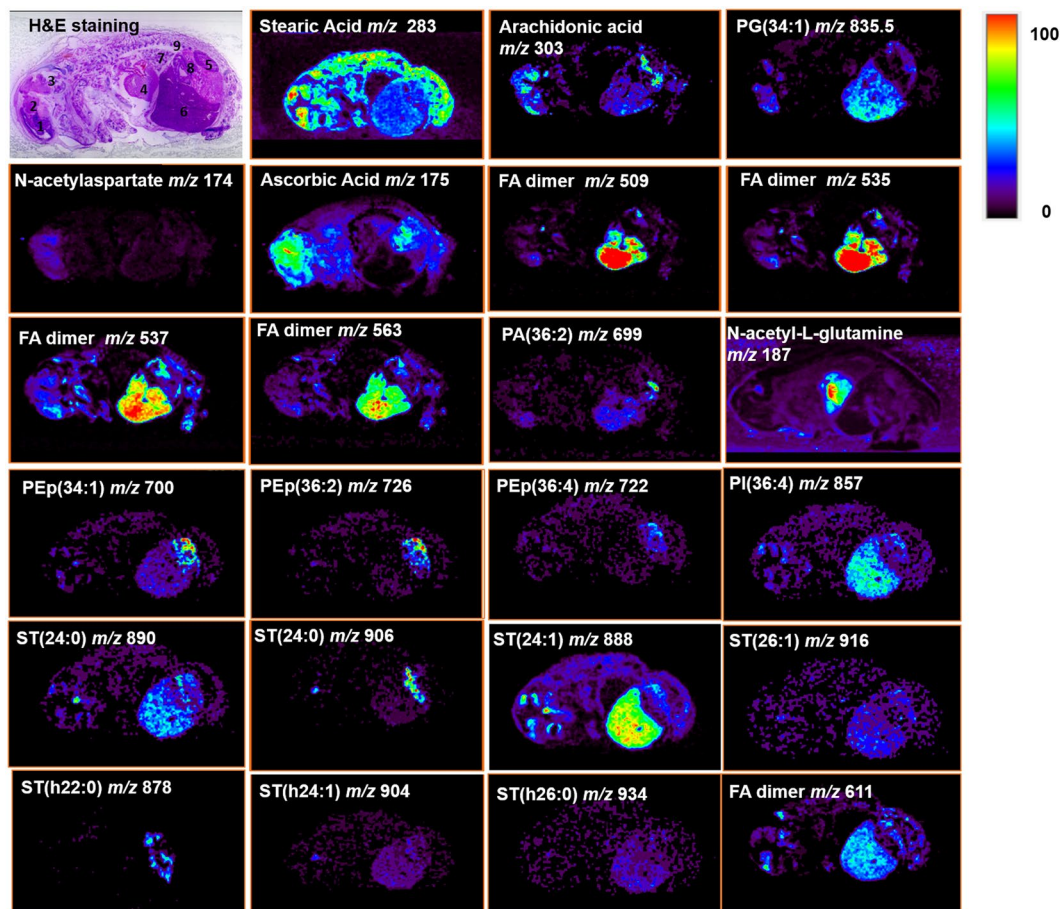


Figure 6. The first figure is an H&E micrograph with numbers indicating the organ location: 1. Proencephalon, 2. Mencephalon, 3. Rhombencephalon, 4. Heart, 5. Kidney, 6. Liver 7. Lungs, 8. Digestive system. The selected ion images show the distribution of specific free fatty acids, metabolites and lipids in the fetus whole body. Abundance in each ion image is independently scaled to 100 using the jet color-scale. Attributions are listed in Table 1. All ions are deprotonated versions of the molecules, viz. $[M - H]^-$, except for PC lipids which were detected as chlorine adducts $[M + Cl]^-$.

Conclusion

Small molecules detected by DESI-MS in tissue sections from whole swine fetuses showed organ-specific distributions, such as N-acetyl-glutamine in the heart, ST(ht22:0) in the intestines, PA(36:2) in the liver, and a number of PS lipids in the nervous system. The chemical information provided by DESI-MS imaging reflects physiology, adds complementary information to anatomical studies and indicates key lipids related to physiological organogenesis. We envisage that this approach can be used to understand inborn developmental errors, especially as related to rare congenital conditions, environmental and epigenetic factors, and due to the application of specific biotechnologies, such as nuclear transfer.

Data Availability

The datasets generated during and/or analyzed during the current study are available from the corresponding author upon request.

References

- Bendixen, E., Danielsen, M., Larsen, K. & Bendixen, C. Advances in porcine genomics and proteomics—a toolbox for developing the pig as a model organism for molecular biomedical research. *Briefings Funct. Genomics Proteomics* **9**, 208–219 (2010).
- Falasca, M. *et al.* The role of phosphoinositide 3-kinase C2 α in insulin signaling. *J. Biol. Chem.* **282**, 28226–28236 (2007).
- van der Veen, J. N., Lingrell, S. & Vance, D. E. The membrane lipid phosphatidylcholine is an unexpected source of triacylglycerol in the liver. *J Biol Chem* **287**, 23418–23426 (2012).
- Lloyd-Evans, E. *et al.* Niemann-Pick disease type C1 is a sphingosine storage disease that causes deregulation of lysosomal calcium. *Nat. Med.* **14**, 1247–1255 (2008).
- Choudhury, A. *et al.* Rab proteins mediate Golgi transport of caveola-internalized glycosphingolipids and correct lipid trafficking in Niemann-Pick C cells. *J. Clin. Invest.* **109**, 1541–1550 (2002).
- Brady, R. O., Johnson, W. G. & Uhlendorf, B. W. Identification of heterozygous carriers of lipid storage diseases. *Am. J. Med.* **51**, 423–431 (1971).
- Steenbergen, R. *et al.* Disruption of the phosphatidylserine decarboxylase gene in mice causes embryonic lethality and mitochondrial defects. *J. Biol. Chem.* **280**, 40032–40040 (2005).

8. Wang, L., Magdaleno, S., Tabas, I. & Jackowski, S. Early embryonic lethality in mice with targeted deletion of the CTP: phosphocholine cytidyltransferase α gene (Pcyl1a). *Mol. Cell. Biol.* **25**, 3357–3363 (2005).
9. Wu, G., Aoyama, C., Young, S. G. & Vance, D. E. Early embryonic lethality caused by disruption of the gene for choline kinase α , the first enzyme in phosphatidylcholine biosynthesis. *J. Biol. Chem.* **283**, 1456–1462 (2008).
10. Merolli, A. & Santin, M. Role of phosphatidyl-serine in bone repair and its technological exploitation. *Molecules* **14**, 5367–5381 (2009).
11. Ross, I. A. *et al.* Free fatty acids profile of the fetal brain and the plasma, liver, brain and kidneys of pregnant rats treated with sodium arsenite at mid-organogenesis. *Toxicol. Ind. Health* **26**, 657–666 (2010).
12. Lo Vasco, V. R. Phosphoinositide pathway and the signal transduction network in neural development. *Neurosci. Bull.* **28**, 789–800 (2012).
13. Zurashvili, T. *et al.* Interaction of PDK1 with Phosphoinositides Is Essential for Neuronal Differentiation but Dispensable for Neuronal Survival. *Mol. Cell. Biol.* **33**, 1027–1040 (2013).
14. Wiseman, J. M., Ifa, D. R., Song, Q. & Cooks, G. R. Tissue imaging at atmospheric pressure using desorption electrospray ionization (DESI) mass spectrometry. *Angew Chem Int Ed Engl* **45**, 7188–92 (2006).
15. Wu, C., Dill, A. L., Eberlin, L. S., Cooks, R. G. & Ifa, D. Mass spectrometry imaging under ambient conditions. *Mass Spectrom Rev* **32**, 218–43 (2013).
16. Eberlin, L. S., Ferreira, C. R., Dill, A. L., Ifa, D. R. & Cooks, G. R. Desorption Electrospray Ionization Mass Spectrometry for Lipid Characterization and Biological Tissue Imaging. *Biochem Biophys Acta* **1811**, 946–960 (2011).
17. Eberlin, L. S. *et al.* Nondestructive, histologically compatible tissue imaging by desorption electrospray ionization mass spectrometry. *ChemBiochem* **12**, 2129–32 (2011).
18. Köfeler, H. C., Fauland, A., Rechberger, G. N. & Trötzlmüller, M. Mass spectrometry based lipidomics: An overview of technological platforms. *Metabolites* **2**, 19–38 (2012).
19. Muro, E., Atilla-Gokcumen, G. E. & Eggert, U. S. Lipids in cell biology: how can we understand them better? *Mol. Biol. Cell* **25**, 1819–1823 (2014).
20. Burnum, K. E. *et al.* Spatial and temporal alterations of phospholipids determined by mass spectrometry during mouse embryo implantation. *J. Lipid Res.* **50**, 2290–2298 (2009).
21. Laskowski, D. *et al.* Lipid profile of bovine blastocysts exposed to insulin during *in vitro* oocyte maturation. *Reprod Fertil Dev.* <https://doi.org/10.1071/RD17248>. (2018).
22. Dill, A. L. *et al.* Multivariate statistical differentiation of renal cell carcinomas based on lipidomic analysis by ambient ionization imaging mass spectrometry. *Anal. Bioanal. Chem.* **398**, 2969–2978 (2010).
23. Pirro, V. *et al.* Lipid characterization of individual porcine oocytes by dual mode DESI-MS and data fusion. *Anal. Chim. Acta* **848**, 51–60 (2014).
24. Onjiko, R. M., Moody, S. A. & Nemes, P. Single-cell mass spectrometry reveals small molecules that affect cell fates in the 16-cell embryo. *Proc Natl Acad Sci USA* **112**, 6545–50 (2015).
25. Gonçalves, R. F. *et al.* Analysis and characterisation of bovine oocyte and embryo biomarkers by matrix-assisted desorption ionisation mass spectrometry imaging. *Reprod. Fertil. Dev.* **28**, 293–301 (2016).
26. Jarmusch, A. K. *et al.* Lipid and metabolite profiles of human brain tumors by desorption electrospray ionization-MS. *Proc. Natl. Acad. Sci.* **113**, 1486–1491 (2016).
27. Onjiko, R. M., Morris, S. E., Moody, S. A. & Nemes, P. Single-cell mass spectrometry with multi-solvent extraction identifies metabolic differences between left and right blastomeres in the 8-cell frog (*Xenopus*) embryo. *Analyst* **141**, 3648–56 (2016).
28. Dueñas, M. E., Essner, J. J. & Lee, Y. J. 3D MALDI Mass Spectrometry Imaging of a Single Cell: Spatial Mapping of Lipids in the Embryonic Development of Zebrafish. *Sci. Rep.* **7**, 1–10 (2017).
29. Onjiko, R. M., Plotnick, D. O., Moody, S. A. & Nemes, P. Metabolic Comparison of Dorsal versus Ventral Cells Directly in the Live 8-cell Frog Embryo by Microprobe Single-cell CE-ESI-MS. *Anal. Methods* **9**, 4964–4970 (2017).
30. Perez, J. C., Tata, A., de Campos, M. L., Peng, C. & Ifa, D. R. Monitoring Toxic Ionic Liquids in Zebrafish (*Danio rerio*) with Desorption Electrospray Ionization Mass Spectrometry Imaging (DESI-MSI). *J. Am. Soc. Mass Spectrom* **28**, 1136–1148 (2016).
31. Xiong, X. *et al.* Data processing for 3D mass spectrometry imaging. *J. Am. Soc. Mass Spectrom.* **23**, 1147–1156 (2012).
32. Evans, H. E. & Sack, W. O. Prenatal Development of Domestic and Laboratory Mammals: Growth Curves, External Features and Selected References. *Anat. Histol. Embryol.* **2**, 11–45 (1973).
33. Hyttel, P., Sinowats, F. & Vejlsted, M. *Essential of Domestic Animal Embryologi, Journal of Chemical information and Modeling* (2013).
34. Eberlin, L. S., Ifa, D. R., Wu, C. & Cooks, R. G. Three-dimensional visualization of mouse brain by lipid analysis using ambient ionization mass spectrometry. *Angew Chem Int Ed Engl.* **49**, 873–6 (2010).
35. Murphy, R. C. *Tandem mass spectrometry of lipids: molecular analysis of complex lipids.* (Royal Society of Chemistry, 2015).
36. Chirkovskaia, E. V., Pomazanskaia, L. F. & Krasil'nikova, V. Comparative study of phospholipids in the neurons and glial cells of the brains of mammals, birds and reptiles. *Zh Evol Biokhim Fiziol.* **14**, 225–9 (1978).
37. Pomazanskaia, L. F. & Krasil'nikova, V. Comparative study of the fatty acid makeup of the neuronal and glial cell phospholipids in the brain of reptiles, birds and mammals. *Zh Evol Biokhim Fiziol* **14**, 327–33 (1978).
38. Lostun, D., Perez, C. J., Licence, P., Barrett, D. A. & Ifa, D. R. Reactive DESI-MS Imaging of Biological Tissues with Dicationic Ion-Pairing Compounds. *Anal. Chem.* **87**, 3286–3293 (2015).
39. Uauy, R. & Dangour, A. D. Nutrition in brain development and aging: role of essential fatty acids. *Nutr Rev* **64**, S24–33 (2006AD) (2006).
40. Girod, M., Shi, Y., Cheng, Y. J. & Cooks, R. G. Desorption Electrospray Ionization Imaging Mass Spectrometry of Lipids in Rat Spinal Cord. *J Am Soc Mass Spectrom.* **21**, 1177–89 (2010).
41. Marcucci, F. & Mussini, E. A method for the gas-chromatographic analysis of N-acetyl-aspartic acid in brain. *J Chromatogr.* **25**, 11–4 (1966).
42. Moffett, J. R., Ross, B., Arun, P., Madhavarao, C. N. & Nambodiri, M. A. A. N-Acetylaspartate in the CNS: From Neurodiagnostics to Neurobiology. *Prog Neurobiol.* **81**, 89–131 (2007).
43. Baslow, M. H. N-acetylaspartate in the vertebrate brain: metabolism and function. *Neurochem Res.* **28**, 941–53 (2003).
44. Singh, M. Essential fatty acids, DHA and human brain. *Indian J Pediatr.* **72**, 239–42 (2005).
45. Banerjee, S. *et al.* Diagnosis of prostate cancer by desorption electrospray ionization mass spectrometry imaging of small metabolites and lipids. 6–11, <https://doi.org/10.1073/pnas.1700677114> (2017).
46. Margulis, K. *et al.* Distinguishing malignant from benign microscopic skin lesions using desorption electrospray ionization mass spectrometry imaging. 1–6, <https://doi.org/10.1073/pnas.1803733115> (2018).
47. Zhang, S., Duan, L., He, S., Zhuang, G. & Yu, X. Phosphatidylinositol 3,4-bisphosphate regulates neurite initiation and dendrite morphogenesis via actin aggregation. *Cell Res* **27**, 243–273 (2017).
48. Ueda, Y. The role of phosphoinositides in synapse function. *Mol Neurobiol* **50**, 821–38 (2014).
49. Eberlin, L. S. *et al.* Ambient mass spectrometry for the intraoperative molecular diagnosis of human brain tumors. *Proc Natl Acad Sci USA* **110**, 161 (2013).
50. Zong, H., Verhaak, R. G. W. & Canoll, P. The cellular origin for malignant glioma and prospects for clinical advancements. *Expert Rev Mol Diagn* **12**(4), 383–394 (2012).

51. Sher, R. B. *et al.* A rostrocaudal muscular dystrophy caused by a defect in choline kinase beta, the first enzyme in phosphatidylcholine biosynthesis. *J. Biol. Chem.* **281**, 4938–4948 (2006).
52. Batenburg, J. J., Klazinga, W. & Van Golde, L. M. Regulation of phosphatidylglycerol and phosphatidylinositol synthesis in alveolar type II cells isolated from adult rat lung. *FEBS Lett.* **147**, 171–4 (1982).
53. Hallman, M., Slivka, S., Wozniak, P. & Sills, J. Perinatal Development of Myoinositol Uptake into Lung Cells: Surfactant Phosphatidylglycerol and Phosphatidylinositol. *Synth. Rabbit.* **20**, 179–185 (2002).
54. Sozo, F., Ishak, N., Bhatia, R., Davis, P. G. & Harding, R. Surfactant phospholipid composition of gastric aspirate samples differs between male and female very preterm infants. *Pediatr. Res.* **82**, 839–849 (2017).
55. Acosta Díaz, R., Arronte Millo, J. & Cabrera Domínguez, N. Evaluación del surfactante en el síndrome de dificultad respiratoria del prematuro. *Rev. Cubana Pediatr.* **72**, 287–294 (2000).
56. Freddi, N. A., Proença Filho, J. O. P. & Fiori, H. H. Terapia com surfactante pulmonar exógeno em pediatria. *J. Pediatr. (Rio. J.)* **79**, S205–S212 (2003).
57. Sánchez-Mendiola, M., Martínez-Natera, O. C., Herrera-Maldonado, N. & Ortega-Arroyo, J. Estudio controlado del tratamiento de la enfermedad de membrana hialina del recién nacido pretérmino con surfactante pulmonar exógeno (porcino vs. bovino). *Gac. Med. Mex.* **141**, 267–271 (2005).
58. Flinders, B. *et al.* Cross-Species Molecular Imaging of Bile Salts and Lipids in Liver: Identification of Molecular Structural Markers in Health and Disease. *Anal Chem* **90**, 11835–11846 (2018).
59. Inglesse, P. *et al.* Deep learning and 3D-DESI imaging reveal the hidden metabolic heterogeneity of cancer. *Chem. Sci.* **8**, 3500–3511 (2017).
60. Pirro, V., Eberlin, L. S., Oliveri, P. & Cooks, R. G. Interactive hyperspectral approach for exploring and interpreting DESI-MS images of cancerous and normal tissue sections. *Analyst* **137**, 2374–2380 (2012).
61. Wu, C., Ifa, D. R., Manicke, N. E. & Cooks, R. G. Molecular imaging of adrenal gland by desorption electrospray ionization mass spectrometry. *Analyst* **135**, 28–32 (2010).
62. Woolman, M. *et al.* Rapid determination of the tumour stroma ratio in squamous cell carcinomas with desorption electrospray ionization mass spectrometry (DESI-MS): a proof-of-concept demonstration. *Proc Natl Acad Sci USA* **110**, 1611–1616 (2013).
63. Eberlin, L. S. DESI-MS Imaging of Lipids and Metabolites from Biological Samples. *Methods Mol Biol.* **1198**, 299–311 (2014).
64. Manicke, N. E. *et al.* Imaging of Lipids in Atheroma by Desorption Electrospray Ionization Mass Spectrometry. *Anal Chem.* **81**, 8702–8707 (2009).

Acknowledgements

Marisol León was supported by Post-Graduation Program at the School of Veterinary Medicine and Animal Science, University of Sao Paulo. The DESI-MS imaging data acquisition was carried out with support from the Indiana Clinical and Translational Sciences Institute funded, in part by Award Number UL1TR002529 from the National Institutes of Health, National Center for Advancing Translational Sciences, Clinical and Translational Sciences Award. The content is solely the responsibility of the authors and does not necessarily represent the official views of the National Institutes of Health.

Author Contributions

M.L.C. wrote the main manuscript text and prepared all the figures. C.R.F. and L.S.E. handled the samples, acquired all DESI-2D data, and were involved in the manuscript preparation. A.K.J. acquired and processed high mass resolution data to identify lipids and metabolites. V.P. coordinated the interdisciplinary team, and performed some of the data processing and manuscript writing. A.C.B.R. performed some of the data processing and manuscript writing on the morphological analysis. P.O.F. was responsible for the morphological analysis reported at the supplementary materials M.A.M. and R.G.C. advised the team and were involved in manuscript writing. All authors reviewed the manuscript.

Additional Information

Supplementary information accompanies this paper at <https://doi.org/10.1038/s41598-019-43698-2>.

Competing Interests: The authors declare no competing interests.

Publisher's note: Springer Nature remains neutral with regard to jurisdictional claims in published maps and institutional affiliations.



Open Access This article is licensed under a Creative Commons Attribution 4.0 International License, which permits use, sharing, adaptation, distribution and reproduction in any medium or format, as long as you give appropriate credit to the original author(s) and the source, provide a link to the Creative Commons license, and indicate if changes were made. The images or other third party material in this article are included in the article's Creative Commons license, unless indicated otherwise in a credit line to the material. If material is not included in the article's Creative Commons license and your intended use is not permitted by statutory regulation or exceeds the permitted use, you will need to obtain permission directly from the copyright holder. To view a copy of this license, visit <http://creativecommons.org/licenses/by/4.0/>.

© The Author(s) 2019